11th ANKARA INTERNATIONAL AEROSPACE CONFERENCE AIAC-2021-064
8-10 September 2021 - METU, Ankara TURKEY

DESIGN OPTIMIZATION OF VARIABLE STIFFNESS COMPOSITE LAMINATES USING SURROGATE MODELS FOR MINIMUM COMPLIANCE OF CURVED WING PANELS

Hasan İnci[1]
TÜBİTAK-SAGE
Ankara, Turkey

Altan Kayran[2]
Middle East Technical University
Ankara, Turkey

ABSTRACT

In this study, variable stiffness curved wing panels are optimized for minimum compliance using surrogate models. With the advance of improved manufacturing capabilities, designers have the ability to design more complex shape and efficient composite structures. In the past three decades, variable stiffness (VS) composite laminates are introduced to the literature. Variable stiffness composites have definite advantages over straight fiber laminates because of the high number of design alternatives they offer. In this study, a curved wing panel is optimized for minimum compliance. To reduce the cost of the design optimization of curved VS composite laminate, a surrogate model is generated from the results of finite element analysis (FEA) in the optimization process, and optimizations are performed with the surrogate model. The reference fiber path definition is determined analytically over the curved composite wing skin panel. The three variables used in the reference fiber path definition are optimized for minimum compliance of the curved wing panel by incorporating the minimum curvature and Tsai-Wu failure constraints.

INTRODUCTION

In advanced composite manufacturing, Automated Fiber Placement (AFP), Automated Tape Laying (ATL) and Continuous Tow Shearing (CTS) methods allowed the design of VS composites with curvilinear fiber paths resulting in the modification of load paths and more favorable stress distribution. In the design of VS composites, iterative optimization methods are used together with FEA to determine the optimum values of the design variables defining the reference fiber path. Many studies have been made on the design optimization of variable stiffness composites with different structural performance requirements such as buckling capacity [Hyer and Lee 1991, Setoodeh et al. 2008], elastic behavior [Gürdal and Olmedo 1993], stiffness [Setoodeh et al. 2006], compressive buckling and first ply failure [Lopes et al. 2008], maximum fundamental frequency [Blom et al. 2008], post buckling progressive damage [Lopes et al. 2007]. Variable stiffness composite design also ensures flexibility for trade-off between different structural properties [Gürdal et al. 2008]. Use of FEA analysis for function evaluations in the optimization process increases the time required in

[1] Senior Researcher, Email: hasan.inci@tubitak.gov.tr
[2] Prof. in Aerospace Engineering, Email: akayran@metu.edu.tr

design optimization studies substantially. Therefore, surrogate models are often used to reduce the optimization time [Nik, et.al. 2014].
In the present study, surrogate models are developed to be used in function evaluations, for the optimization of variable stiffness composite laminates. The surrogate models which are developed in the present study are based on Radial Basis Functions (RBF) approximation [Broomhead and Lowe 1998]. Optimizations with the surrogate models are performed by the Particle Swarm Optimization (PSO) [Shi and Eberhart 1998] and Whale Optimization Algorithms (WOA) [Mirjalili and Lewis, 2016]. Compliance minimization of the curved variable stiffness composite laminate is performed. The loading of the curved composite laminate panel is extracted from a real wing structure which is loaded from its wing tip. The projected reference fiber path definition is a third order polynomial for flat plates. This polynomial is combined with the wing surface equations to obtain a mathematical expression for the reference fiber path definition on the curved wing surface.
Results for both PSO and WOA are presented to guarantee the global optimum. Also the same loads are used to optimize a flat composite plate with the same stacking to guarantee the performance of the newly implemented fiber path definition.
Optimization results for minimum compliance of curved composite win panel with the manufacturing and Tsai-Wu failure constraints are presented.

METHOD

In the current study, design optimization of VS curved composite wing panels is performed using surrogate models to reduce the computational cost of optimization. Compliance minimization is performed on an aircraft wing box model for the upper root composite skin panel. Wing box geometry is created with 5 stations with NACA 4412 airfoil cross section. The total chord length of the wing is 1 m. The front spar is located at 20% of the chord; rear spar is located at 70% of the chord with respect to the leading edge of the wing. The half span of the wing is 2.5 m with five stations and 6 ribs each located 0.5 m away from each other. Since the main load carrying part of the wing is the wing box, only the wing box portion of the wing is used in the analysis. Leading edge and trailing edge portions of the wing is not taken into account. The resultant wing geometry is shown in Figure 1 and Figure 2.

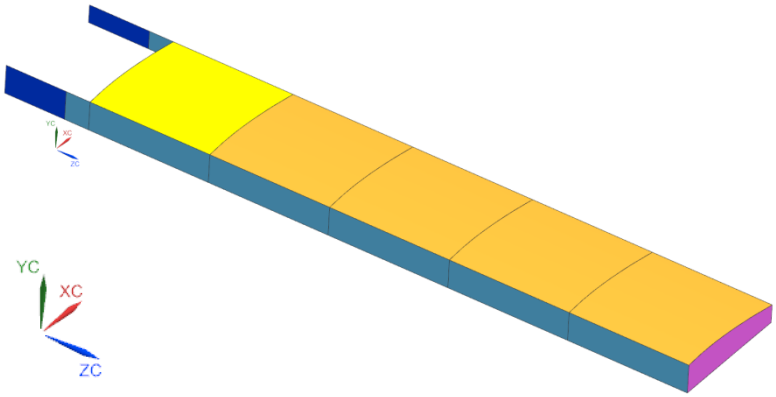

Figure 1: Wing geometry and material assignments for the wing box geometry

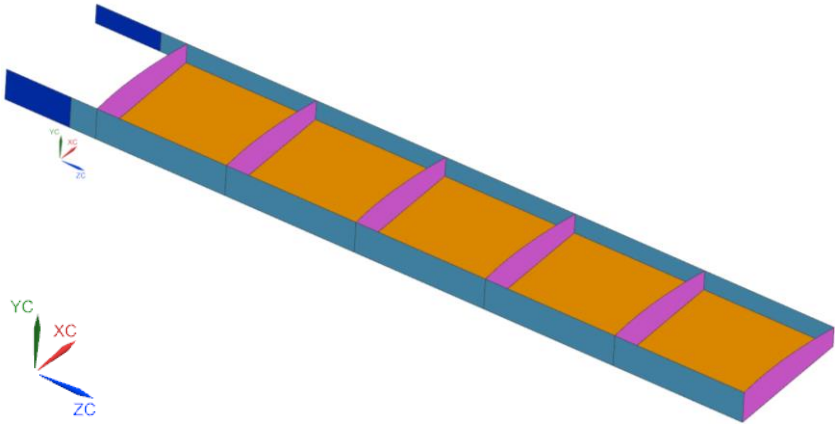

Figure 2: Wing box geometry, upper skin panels removed

The wing box geometry is created with surfaces. In Figure 1, blue parts are aluminum spars with 10 mm thickness, pink parts are aluminum ribs with 3 mm thickness. The orange curved panels and the yellow panel are composite curved skin panels both on the upper and lower surfaces. Composite panels are 3 mm thick with 24 mid-plane symmetric plies. Stacking of the composites is taken as $[(+\theta/-\theta)_6]_s$. Particularly, in Figure 1 the yellow panel is highlighted because it is designated as the critical panel to be optimized. Variable Stiffness (VS) laminate is defined with a novel fiber path definition over the curved surface.

The design optimization is performed over the curved panel at the inboard section of the wing indicated in yellow color in Figure 1, since upward bending load creates a critical compression condition for the particular skin panel. The edge loadings acting on the panel are extracted from the full wing model. Edge loadings and boundary conditions are defined to match the behavior of the full wing model.

Design optimization is performed with a surrogate model. The surrogate model is based on Radial Basis Function (RBF) approximation. For the optimization algorithm, two optimization algorithms are employed to guarantee the global optimum. For this purpose, Particle Swarm Optimization (PSO) and Whale Optimization Algorithms (WOA) are developed. Surrogate model generation and optimizer codes are coupled with NASTRAN finite element solver. Surrogate model is created utilizing the finite element solutions corresponding to for some number of analysis points decided based on design of experiments. Following the check of the error metrics are for the surrogate model, developed surrogate model is sent to the optimizers and optimizations are performed by the surrogate model. The curved panel optimization definition has two constraints. The first constraint is the manufacturing constraint, taken from the maximum curvature constraint of the manufacturing machines. The second constraint is the failure constraint of the curved composite panel. Under the given load condition, the composite laminate should not fail; hence the design-optimization process should provide a safe design. Since the optimization is performed with the surrogate model, the failure response is necessary for the constraint calculations. In this respect, during the surrogate model generation, along with the compliance response approximation, approximate model for the failure index response is also created with the same procedure as the compliance response of the plate. The optimized results are compared with the finite element solution for the specified design variable inputs. By comparing the optimization results obtained with the surrogate models with the finite element solutions for the specified design variable inputs, performance of both optimizers are checked and the global optimum is guaranteed.

The aforementioned concepts are explained briefly in the proceeding sections.

Reference Fiber Path Definition

Equation (1) gives the x and y coordinates of the upper (x_U, y_U) and lower (x_L, y_L) surfaces of the wing; hence the thickness distribution of the symmetric airfoil without camber. "y_t" is the

symmetrical half thickness distribution of the airfoil for both upper and lower surfaces of the airfoil, as measured perpendicular to the mean camber itself. "y_c" is the y coordinate of the mean camber line of the cambered airfoil geometry, as given in Equations (2) and (3). All equations are presented for a unit chord length airfoil. In all equations "c" states the chord length of the airfoil, "x" is the position along the chord from 0 to c, "t" is the maximum thickness of the airfoil as the percent of the chord designated by the last two digits of the NACA-4 Series designation, "m" is the maximum camber as the percent of the chord given by the first digit of the NACA-4 Series designation, "p" is the location of the maximum camber along the chord in tenths of chord and it given by the second digit of the designation. Equation (1) shows that the upper and lower surfaces of the wing geometry have different equations because of the camber. If the maximum camber "m" is zero, then upper and lower surfaces of the wing have the same "y" coordinates implying symmetric airfoil. It should be noted that the tangent angle "θ" in Equation (1) is given by Equations (4) and (5).

$$x_U = x - y_t sin\theta, \quad x_L = x + y_t sin\theta, \quad y_U = y_c + y_t cos\theta, \quad y_L = y_c - y_t cos\theta \tag{1}$$

$$y_t = 5t\left[0.2969\sqrt{\frac{x}{c}} - 0.1260\left(\frac{x}{c}\right) - 0.3516\left(\frac{x}{c}\right)^2 + 0.2843\left(\frac{x}{c}\right)^3 - 0.1015\left(\frac{x}{c}\right)^4\right] \tag{2}$$

$$y_c = \begin{cases} \frac{m}{p^2}\left(2p\left(\frac{x}{c}\right) - \left(\frac{x}{c}\right)^2\right), & 0 \le x \le pc \\ \frac{m}{(1-p)^2}\left((1-2p) + 2p\left(\frac{x}{c}\right) - \left(\frac{x}{c}\right)^2\right), & pc \le x \le c \end{cases} \tag{3}$$

$$\theta = arctan\left(\frac{dy_c}{dx}\right) \tag{4}$$

$$\frac{dy_c}{dx} = \begin{cases} \frac{2m}{p^2}\left(p - \frac{x}{c}\right), & 0 \le x \le pc \\ \frac{2m}{(1-p)^2}\left(p - \frac{x}{c}\right), & pc \le x \le c \end{cases} \tag{5}$$

In the present study, wing structure that is studied has NACA 4412 airfoil geometry. Utilizing Eqns. 1-5, sample NACA 4412 airfoil geometry is generated such that "chordwise" and "thickness" directions correspond to x-axis and y-axis, respectively. It should be noted present design optimization study can be performed for any general curved panel that has an analytical surface definition.

To generate a 3D wing skin structure with the NACA 4412 airfoil, splines created, utilizing the uppe (x_U, y_U) and lower airfoil (x_L, y_L) coordinates, are extruded along the span of the wing. Hence with this method, the two surfaces, $\varphi_1(x_U, y_U, z)$ and $\varphi_2(x_L, y_L, z)$are created for the upper and lower surfaces of the airfoil. Figure 3 shows the generated wing geometry used in the present study.. In Figure 3, "chord", "thickness", "span" axes correspond to x, y and z, respectively for the global coordinate system.

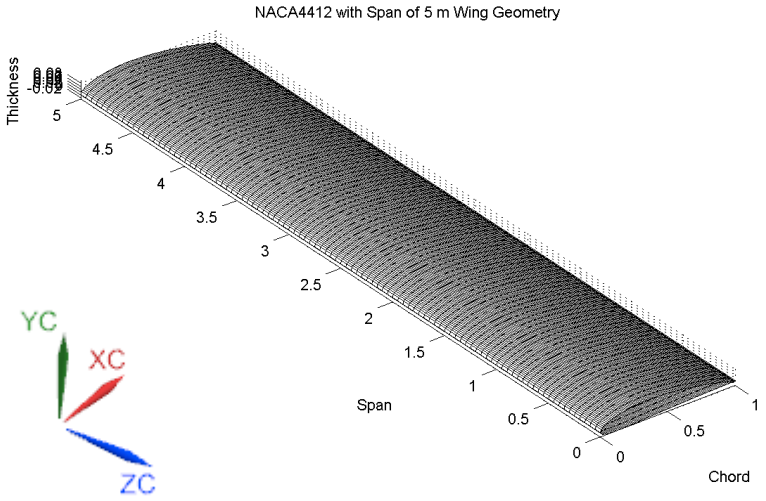

Figure 3 - NACA 4412 wing geometry with 1m of chord length and 5m of span

In this study, for the curvilinear fiber paths, a cubic polynomial is suggested as given by Eqn. (6). Equation (6) is written with respect to the global axis system x,y,z. The fiber paths are created in the x-z plane of the 3D space, which is the projected chord-span plane, via Eqn. (6). Equation (6) returns the contours of the fiber paths not the fiber angles at the points. Equation (7) gives the fiber angles at each coordinate, and fiber paths are drawn with utilizing Eqn. (6). In the present study, constants "$\overline{a}$", "$\overline{b}$" and "$\overline{c}$" are the variables, where "$\overline{a}$" is equal to "3a", "$\overline{b}$" is equal to "2b" and "$\overline{c}$" is equal to "c", in the optimization problem and reference fiber path definition changes according to the changes in the coefficients of the cubic polynomial.

$$x(z) = az^3 + bz^2 + cz + d \qquad (6)$$

$$\frac{dx}{dz} = tan(\theta), \quad \theta = \arctan\left(\overline{a}z^2 + \overline{b}z + \overline{c}\right) \qquad (7)$$

Individual fibers are assumed to be placed with the shifted fiber path method [Gürdal and Olmeda, 1993]. This method shifts the fiber paths in the "chord" axis x, and for the same z-coordinate, fiber angles do not change.

Once the fiber paths are defined in the x-z plane, one needs to modify these paths to follow the airfoil surface. For the calculation of the height of the airfoil surface, x-coordinates are necessary and these points are gathered from Eqn. (6). Once the necessary x-coordinates are obtained, these points are substituted into Eqns. (1)-(5) for the calculation of the thickness coordinates y_U and y_L.Fiber paths generated follow the airfoil geometry as seen in Figure 4.

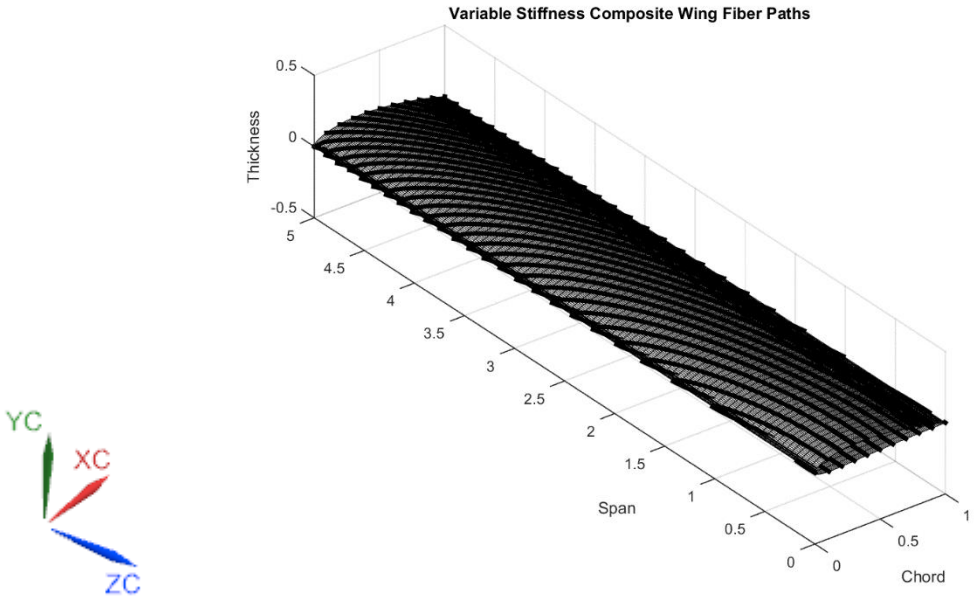

Figure 4 - Fiber paths on the airfoil geometry

Radial Basis Functions (RBF) Approximation

Because of the high computational cost of FEA in each iteration of the optimization process, surrogate models are decided to be used for function evaluations of the optimization to reduce the analysis time. From the literature it is seen that surrogate models based on RBF approximation with multiquadric basis functions yield satisfactory results for VS composite laminate optimizations. [Nik, et.al. 2014]

Radial basis function approach constructs a linear space which depends on the position relative to the known data points according to an arbitrary distance measure [Broomhead and Lowe 1988]. The basis functions, which are generally nonlinear, are introduced as $\psi(\|x - x_i\|)$, where ψ is a different basis function depending on the problem, $\|x - x_i\|$ is the Euclidian distance of the two sample data points. Radial basis function approach creates linear space between the basis functions. Approximation of a function by the radial basis functions can be written as,

$$\tilde{y}(x) = \sum_{i=1}^{n} w_i \, \psi(\|x - x_i\|) \tag{8}$$

where $\tilde{y}$ is the approximate value of the objective function in an optimization problem and w_i is the weight of the basis function evaluated by fitting the model to the training data. This results in a linear system of equations given by,

$$\boldsymbol{y} = \boldsymbol{\psi w} \tag{9}$$

where $\boldsymbol{y}$ is the vector of function values at the training data, $\boldsymbol{w}$ is the vector of basis function weights and $\boldsymbol{\psi}$ is a matrix, which consists of Euclidian distance of each training data with respect to one another, also called the Gramian matrix. Matrix $\boldsymbol{\psi}$ is defined by,

$$\boldsymbol{\psi} = \begin{bmatrix} \psi(x_1.x_1) & \psi(x_1.x_2) & \dots & \psi(x_1.x_n) \\ \psi(x_2.x_1) & \psi(x_2.x_2) & \dots & \psi(x_2.x_n) \\ \vdots & \vdots & \ddots & \vdots \\ \psi(x_n.x_1) & \psi(x_n.x_2) & \dots & \psi(x_n.x_n) \end{bmatrix} \tag{10}$$

where *n* is the number of sample data used for the interpolation. Once Eqn. (9) is solved for $\boldsymbol{w}$, the weights of the approximate function are obtained. The size of the weight vector obtained is same as the number of sample points. This is a strict interpolation in which the approximate equation satisfies the sampling points exactly. Having obtained the weights, one can then evaluate Eqn. (8) for the value of the approximate function for any arbitrary point different from the sampling points. For RBF approximations, multiquadric basis functions are generally used as given in Eqn. (11),

$$\psi = \sqrt{r^2 + s^2} \tag{11}$$

where *r* is the Euclidian distance between points and *s* is the width parameter which is chosen a value in the interval [0,1]. It should be noted that design variables are also scaled to fit into the [0,1] interval [Nik, et.al. 2014].

In this study, surrogate models for the compliance response and failure index response of the composite laminates are developed. Surrogate models are developed by performing function evaluations at the sampling points. Large set of sample points are used to ensure the accurate performance of the surrogate model, and while selecting the sample points, Latin Hypercube Sampling is used instead of random sampling for better coverage. Weights of the basis functions are calculated from the sample points by FEA. It is seen that surrogate models have very good performance in determining the optimum parameters of the reference fiber paths for the present study.

Particle Swarm Optimization (PSO)

For the purposes of the study, an optimizer, based on Particle Swarm Optimization (PSO) algorithm, is developed. PSO simulates the behavior of a school of birds. Each individual is named as a "particle" which, in fact, represents a potential solution to a problem. Each particle is treated as a point in a D-dimensional space and adjusts its flying according to its own flying experience and its companions' flying experience. The *i*th particle is represented as $X_i = (x_{i1}, x_{i2}, \dots, x_{iD})$. The best previous position (the position giving the best fitness value) of any particle is recorded and represented as $P_i = (p_{i1}, p_{i2}, \dots, p_{iD})$. The index of the best particle among all the particles in the population is represented by the symbol *g*. The rate of the position change (velocity) for particle *i* is represented as $V_i = (v_{i1}, v_{i2}, \dots, v_{iD})$. The particles are manipulated according to Equations (10) and (11),

$$v_{id} = w * v_{id} + c_1 * rand( ) * (p_{id} - x_{id}) + c_2 * rand( ) * \left(p_{gd} - x_{id}\right) \tag{10}$$

$$x_{id} = x_{id} + v_{id} \tag{11}$$

where c_1 and c_2 are two positive constants, rand( ) is a random function in the range [0,1], *w* is the inertia weight which reduces linearly as the iteration goes on. Inertia weight is usually taken between [0.9, 0.4] [Shi and Eberhart 1998]. The first part of the Eqn. (10) lets the particles to move in the search space globally with the inertia weight. The second part of the Eqn. (10) is the "cognition" part, which represents the private thinking of the particle itself. The third part is the "social" part, which represents the collaboration among the particles. Equation (10) is used to calculate the particle's new velocity according to its previous velocity and the distances of its current position from its own best experience (position) and the group's best experience. Then, the particle flies toward a new position according to Eqn. (11). The performance of each particle is measured according to a predefined fitness function, which is related to the problem to be solved.

Manufacturing and failure constraints are checked for constraint violation and the objective function is penalized if constraint violation is encountered. Termination condition of the

optimization process is based on a prescribed tolerance which is calculated utilizing the Euclidian distance of each particle with respect to the best particle in the population. This approach guarantees that all the population is gathered at the optimum point. The average distance of the stopping criteria is taken as 0.001 and maximum number of iterations is selected as 700.

Whale Optimization Algorithm (WOA)

WOA is a recently developed heuristic optimization algorithm, inspired by the bubble-net hunting strategy of humpback whales [Mirjalili and Lewis, 2016]. Algorithm simulates the hunting behavior with random or the best search agent (individual in the population) to chase the prey and the use of a spiral to simulate the bubble-net attacking mechanism of humpback whales. It has been observed that hunting is done by creating distinctive bubbles along a circle or '9'-shaped path [Mirjalili and Lewis, 2016].

WOA assumes that the current best candidate solution is close to the optimum. After defining the best agent, other search agents update their positions toward the best search agent. This is the exploitation phase of the algorithm. The mathematical background of the algorithm is given by Eqns. (12) through (16).

$$\vec{X}(t+1) = \begin{cases} \overrightarrow{X^*}(t) - \vec{A} \cdot \vec{D} & if\ p < 0.5 \\ \overrightarrow{D'} \cdot e^{bl} \cdot cos(2\pi l) + \overrightarrow{X^*}(t) & if\ p \geq 0.5 \end{cases} \quad (12)$$

In Eqn. (12), t indicates the current iteration, $\vec{A}$ and $\vec{C}$ are the coefficient vectors given by Eqns. (15) and (16), $\overrightarrow{X^*}$ is the position vector of the best solution obtained so far, $\vec{X}$ is the position vector, $\vec{D}$ and $\overrightarrow{D'}$ vectors are the distance vectors defined for two different position update mechanisms and they are given by Eqns. (13) and (14), | | denotes the absolute value, · denotes the element-by-element multiplication operator, *p* is a random number in the range [0,1], *l* is a random number vector in the range [−1,1], *b* is a constant for defining the shape of the logarithmic spiral. In the WOA, $\overrightarrow{X^*}$ is updated in each iteration if there is a better solution. As given in Eqn. (12), if *p* is less than 0.5, the algorithm applies the *Shrinking encircling mechanism*, or else the algorithm applies the *Spiral updating position*.

$$\vec{D} = \left|\vec{C} \cdot \overrightarrow{X^*}(t) - \vec{X}(t)\right| \quad (13)$$

$$\overrightarrow{D'} = \left|\overrightarrow{X^*}(t) - \vec{X}(t)\right| \quad (14)$$

For the exploration phase of the algorithm $\overrightarrow{X^*}(t)$ is replaced by the position of a random search agent if $|\vec{A}| > 1$.

$$\vec{A} = 2\vec{a} \cdot \vec{r} - \vec{a} \quad (15)$$

$$\vec{C} = 2 \cdot \vec{r} \quad (16)$$

In Eqns. (15) and (16), $\vec{a}$ is linearly decreased from 2 to 0 over the course of iterations (in both exploration and exploitation phases) and $\vec{r}$ is a random vector in the range [0,1]. In the WOA, there are only two internal parameters to be updated; $\vec{A}$ and $\vec{C}$.

WOA stops by the satisfaction of the termination criterion. In the current study, the same initial population generation, termination criterion, maximum number of iteration and tolerance are used as the PSO algorithm. It should be noted that there are no initial velocity definitions for the WOA, unlike PSO.

Load and Boundary Conditions

As stated earlier, the load case of the current study is obtained from analysis of a full wing structure. Full wing structure loading is shown in Figure 5. All components on the wing is modelled with shell elements. Wing is loaded from the lower tip of the spars, as in tip load test and a load of 2500 N is applied to the tip of the front and rear spars. Wing is fixed at its root rib from the edges of the rib at all degrees of freedom and linear static solution is

performed. The resultant loading acting on the upper panel closest to the root is obtained and applied to the curved skin panel.

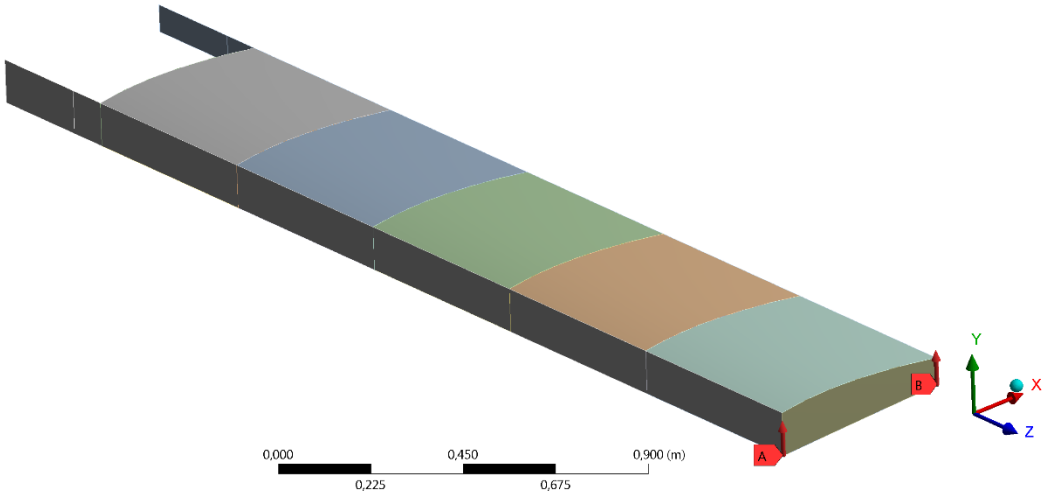

Figure 5 - Geometry and loading of the full wing

The edge loadings read from the full wing analysis are applied to the curved upper wing skin panel. In Table 1, resultant edge loads are shown and Figure 6 shows the edge numberings. Total loads are applied to the edges. These loads are distributed evenly to all nodes lying on the particular edge.

Table 1 - Edge loads applied to the skin panel optimizations

	Edge 1	**Edge 2**	**Edge 3**	**Edge 4**
x-axis (N)	1168,68	-10,53	-1322,47	169,08
y-axis (N)	-376,09	-12,61	405,96	14,47
z-axis (N)	99509,89	-8927,51	-83448,3	-6081,53

For the boundary conditions of the case study, all edge nodes are fixed in y-axis translation and all rotational degrees of freedom except the corner nodes. The corner nodes are fixed in all translational and rotational degrees of freedom. The corresponding finite element model is given in Figure 7 with 2500 elements.

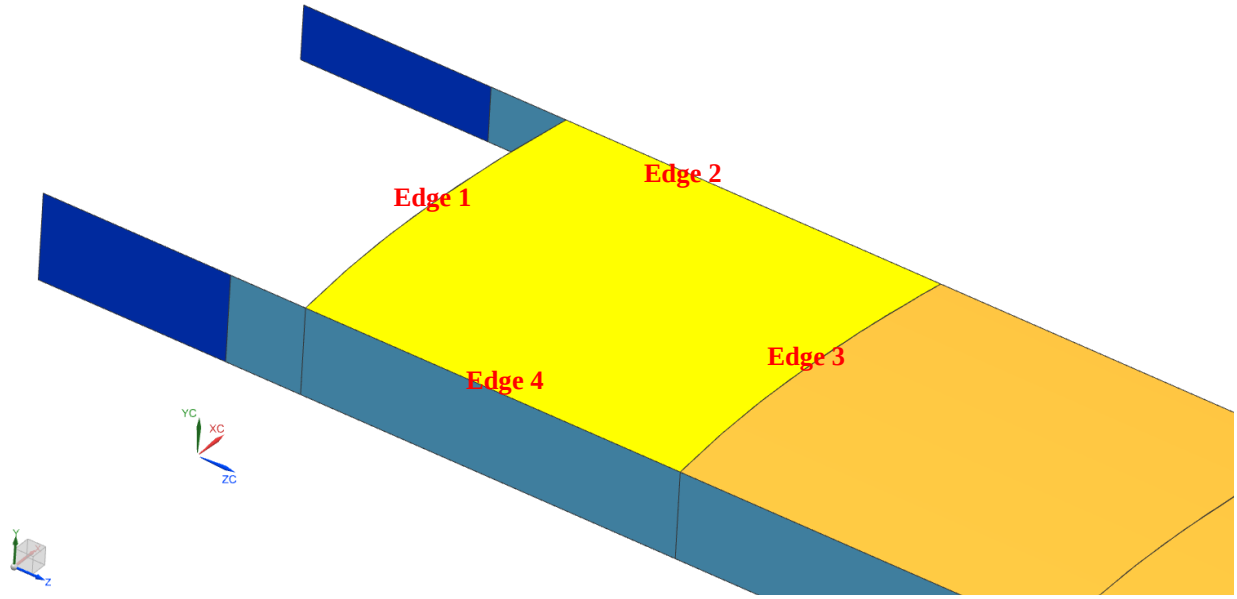

Figure 6 - Edge numberings in the results

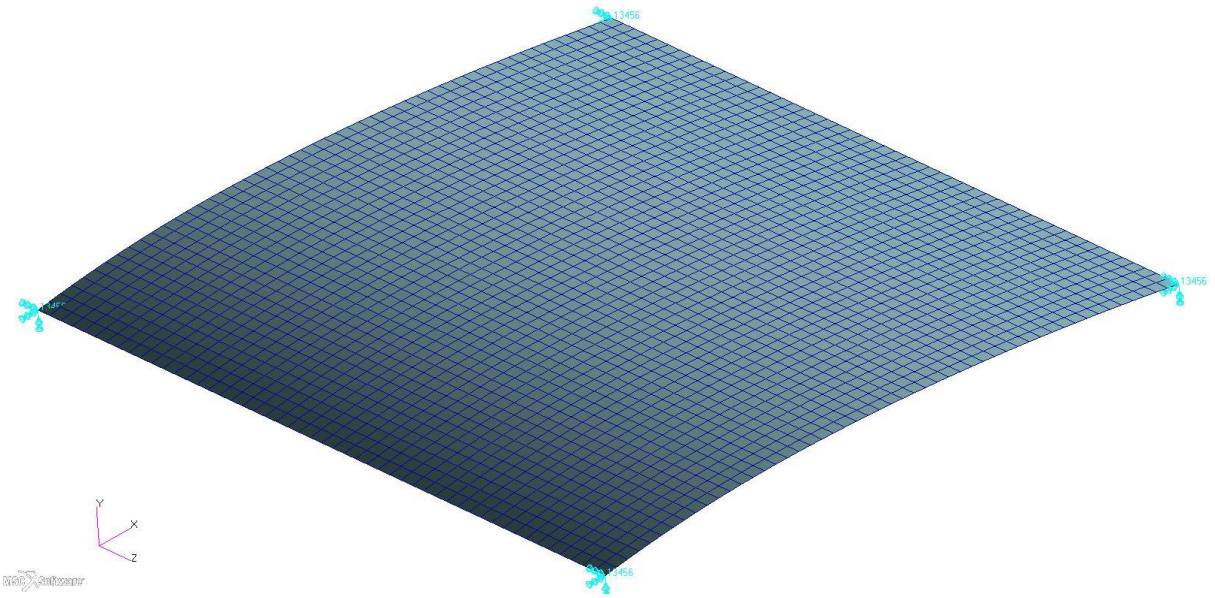

Figure 7 - Finite element model of the skin panel

Origin of the Reference Fiber Path

The origin of the reference fiber path affects the shape of the fiber path; hence the performance of the resulting reference fiber path on the design optimization of the curved panel. The reference fiber path definition is a third order polynomial, as mentioned earlier. The loading condition is nearly symmetric; therefore it is expected to have a symmetric fiber path distribution over the curved skin panel. In this study, it decided to place the reference fiber path origin at the center of the curved plate with respect to x-z plane. Placing the reference fiber path origin at the origin enables to achieve a symmetrical fiber path distribution over the curved skin panel. Origin of the reference fiber path and the corresponding global axes are shown in Figure 8.

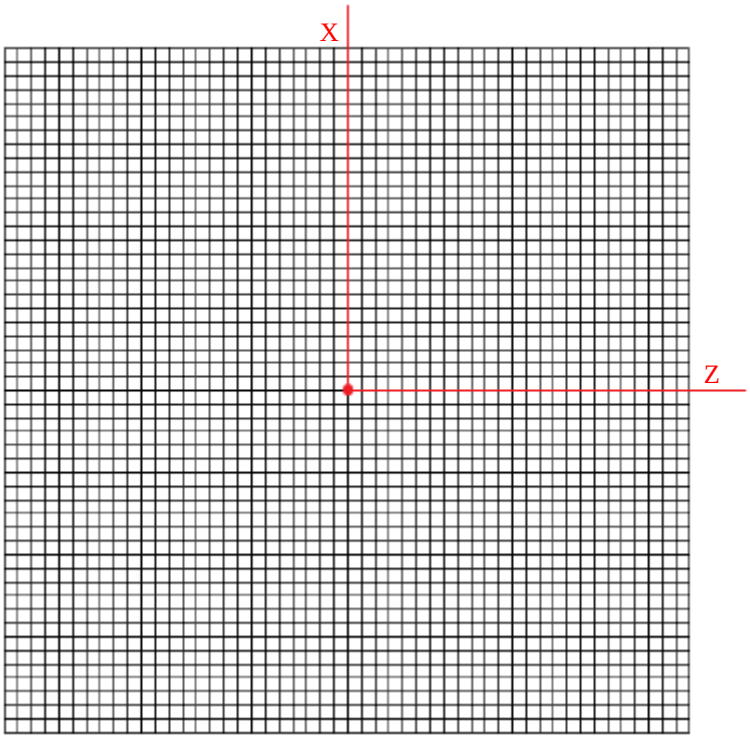

Figure 8 – Origin of the reference fiber path

RESULTS

Performed optimizations are presented in this section which consists of 3 sets of results. First set of results show the optimization of curved panel at the root of the wing in Figure 1 with only manufacturing constraint. Second set of results show the optimization of the flat panel with the same loading and only manufacturing constraint as the curved panel case. The first two set of results are presented to ensure that the fiber path definition and manufacturing constraint are correctly handled. Third set of results show the curved panel optimization with both manufacturing and failure constraints.

Curved and flat panel optimization results, obtained by the PSO and WOA optimizers, are examined and comparisons are made to infer conclusions with regard the accuracy of the optimized reference fiber path definition. The loading of the panels is obtained from the full wing and applied both curved and flat panel. For both panels, there are 2500 elements in the finite element model. Each element has its own property and therefore fiber angle. The variable stiffness plate is obtained by updating fiber angles of each element based on their locations in the panel.

In the current study, each response has a surrogate model. Surrogate models are created with certain number of training points and the surrogate model is built up on the data gathered at the training points. The number of training points is given as “# of train. data” in the results table presented in the proceeding sections. There is also a width parameter for the surrogate model and it is denoted as “Width P.” in the results table. The performance of the surrogate models are tested at some random points designated as control points and denoted by “# of ctrl. pnts.”. At the control points, the error metrics of the surrogate model are evaluated. “Rsquare” is the R^2 error, and “RMSE” is the root mean square error. “S.average” is the average response of the surrogate model at the control points, and it is compared with the RMSE value.

Curved panel optimization with single constraint

For the curved panel with the manufacturing constraint only, optimizations are performed with the surrogate model generated. For the curvilinear fiber path optimization of the curved

panel, compliance response surrogate model parameters and performance metrics are presented Table 2. Surrogate model is generated after some trials on the selected number of training data and the width parameter. Table 2 shows that fits considerably well to the finite element model response, with approximately 8% difference in the RMSE value.

Table 2 - Curvilinear fiber path optimization compliance response surrogate model parameters and performance metrics for the curved panel

# of train. data	**# of ctrl. pnts.**	**Width P.**
600	50	0.2
Rsquare	**RMSE**	**S.average**
0.9387	50.72	609.28

As discussed before, three design variables are used for the reference fiber path definition and these are the coefficients of the x derivative of the cubic polynomial given by Eqn. (7).For the root skin panel studied in this study, the upper boundary is taken as +10 and lower boundary is taken as -10 for the design variables "$\overline{a}$", "$\overline{b}$" and "$\overline{c}$" in Eqn. (7).

Results of Particle Swarm Optimization:

The initial velocities of the particles are given as random for the Particle Swarm Optimization. Ten individual optimization results are given in Table 3. The optimum design variable values are given in Table 3 as "Best Var.". The resulting optimum strain energy is 361.061 J reached in the 5th optimization run. For the curvilinear fiber path optimization with Particle Swarm Optimization. "Best Obj. Val." is the value of the objective function obtained from the surrogate model, "FEA" is the resulting fiber path's finite element analysis solution and "FEA Error" is the error between the surrogate model response and the result obtained by the finite element analysis. Table 3 shows that ten different runs resulted in the same optimum value of the total strain energy, and that surrogate model and finite element results are close to each other with about 1% difference. In 10 individual optimizations, total number of iterations is 4350 in total with 30 function evaluations for each iteration. It is seen that 5th optimization run, which has the highest number of iterations, yielded to the lowest objective value.

Table 3 - Particle Swarm Optimization results for the curvilinear fiber path

RUN		**1**	**2**	**3**	**4**	**5**	**6**	**7**	**8**	**9**	**10**
Max. iter #		430	476	417	447	625	375	431	421	365	363
Best Obj. Val.		361.063	361.063	361.063	361.063	361.061	361.069	361.063	361.063	361.068	361.068
FEA		357.254	357.254	357.254	357.254	357.252	357.259	357.254	357.254	357.258	357.258
FEA Error		1.066%	1.066%	1.066%	1.066%	1.066%	1.066%	1.066%	1.066%	1.066%	1.066%
Best Var.	$\overline{a}$	2.5806	2.5806	2.5806	2.5806	2.5806	2.5804	2.5806	2.5806	2.5803	2.5802
	$\overline{b}$	-7.7475	-7.7475	-7.7475	-7.7475	-7.7475	-7.7478	-7.7475	-7.7475	-7.7476	-7.7479
	$\overline{c}$	-2.7362	-2.7362	-2.7362	-2.7362	-2.7362	-2.7361	-2.7362	-2.7362	-2.7367	-2.7364

Results of Whale Optimization Algorithm:

Unlike the PSO, in WOA there is no parameter to set in the Whale Optimization Algorithm. Ten individual optimization results are given in Table 4. The same nomenclature is used in Table 4 as in Table 3. The resulting optimum total strain energy is obtained as 361.062 J for the curvilinear fiber path optimization with the Whale Optimization Algorithm. As in PSO, in WOA, surrogate model and finite element results are close to each other with almost same difference as in the PSO. However, in WOS, total number of iterations in 10 optimization runs is are 7000 in total with 30 function evaluations for each iteration. In the case, maximum number of iterations is reached in each optimization run, and 7th optimization run yielded to the lowest objective value.

Table 4 - Curvilinear fiber path Whale Optimization Algorithm results for the curvilinear fiber path

RUN		**1**	**2**	**3**	**4**	**5**	**6**	**7**	**8**	**9**	**10**
Max. iter #		700	700	700	700	700	700	700	700	700	700
Best Obj. Val.		361.063	361.069	361.063	361.063	361.063	361.063	361.062	361.063	361.067	361.066
FEA		357.254	357.258	357.254	357.254	357.254	357.254	357.253	357.254	357.256	357.256
FEA Error		1.066%	1.066%	1.066%	1.066%	1.066%	1.066%	1.066%	1.066%	1.066%	1.066%
Best Var.	$\overline{a}$	2.5806	2.5806	2.5806	2.5806	2.5806	2.5806	2.5806	2.5806	2.5806	2.5805
	$\overline{b}$	-7.7475	-7.7475	-7.7475	-7.7475	-7.7475	-7.7475	-7.7475	-7.7475	-7.7473	-7.7473
	$\overline{c}$	-2.7362	-2.7362	-2.7362	-2.7362	-2.7362	-2.7362	-2.7362	-2.7362	-2.7365	-2.7363

It should be noted that both optimizers yield to the same global optimum. The resulting optimum fiber path of the optimizations is given in
Figure **9**. The blue line shows +θ orientation of the fibers, the red line shows –θ orientation of the fibers.

In Figure 9, it is seen that there is a shift in reference fiber path to the root of the panel. The loads obtained from the wing are not exactly symmetric, also the curved panel is not symmetric through curved part. Therefore, it is decided to eliminate one of the factors effecting the symmetry of the reference fiber path. For the next set of study flat composite plate is optimized with the same loading condition. The resultant reference fiber path definition will define the major contributor to the shift of the reference fiber path.

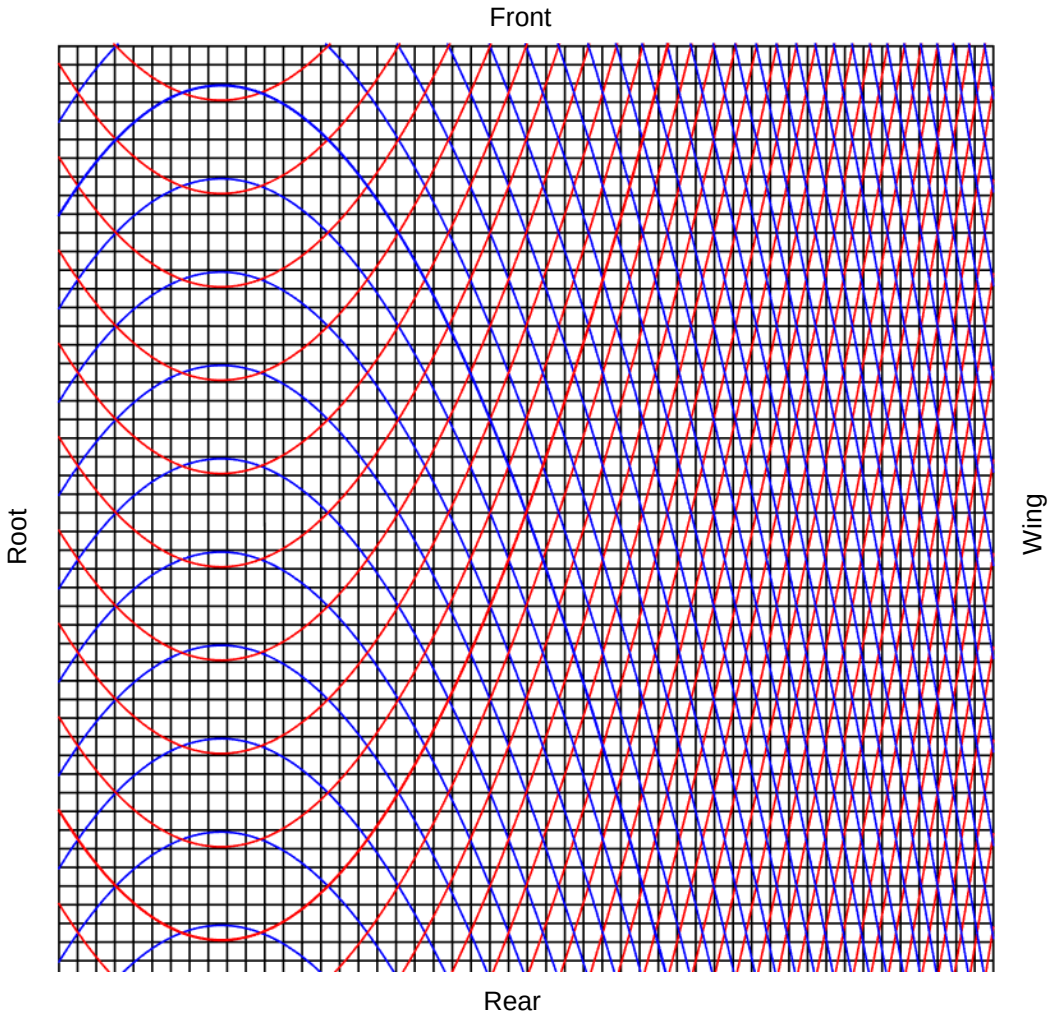

Figure 9 - Resulting curvilinear fiber paths of the curved plate, (top view)

Flat plate optimization with single constraint

Flat plate optimization is performed to check if the optimum fiber path obtained for the curved panel is reasonable or not. Flat plate is obtained by keeping the dimensions of the curved panel and straightening the curved panel. For the curvilinear fiber path optimization of the flat plate with manufacturing constraint, compliance response surrogate model parameters and performance metrics are presented Table 5. Again, surrogate model is generated after some trials on the selected number of training data and the width parameter.

Table 5 – Curvilinear fiber path optimization compliance response surrogate model parameters and performance metrics for the flat plate

# of train. data	**# of ctrl. pnts.**	**Width P.**
600	50	0.05
Rsquare	**RMSE**	**S.average**
0.9524	60.4643	320.9818

Results of Particle Swarm Optimization:

For the flat plate, the optimum strain energy is determined as 241.9811 J for the curvilinear fiber path optimization with Particle Swarm Optimization. In this case, total number of iterations is 4474 iterations in total with 30 function evaluations for each iteration. 5th optimization run yields to the lowest objective value it has the highest number of iterations. It should be noted that there is 2.4% difference between the optimum strain energy obtained utilizing the surrogate model in and the FEA solution for the optimum fiber path. Optimization details are given in Table 6.

Table 6 - Curvilinear fiber path Particle Swarm Optimization Results

RUN		**1**	**2**	**3**	**4**	**5**	**6**	**7**	**8**	**9**	**10**
Max. iter #		442	456	457	437	563	380	472	584	320	363
Best Obj. Val.		241.9811	241.9813	241.9812	241.9816	241.9811	241.9812	241.9818	241.9816	241.9817	241.9811
FEA		247.9930	247.9930	247.9930	247.9930	247.9930	247.9930	247.9930	247.9930	247.9930	247.9930
FEA Error		2.48%	2.48%	2.48%	2.48%	2.48%	2.48%	2.48%	2.48%	2.48%	2.48%
Best Var.	$\overline{a}$	9.2853	9.2853	9.2853	9.2853	9.2853	9.2853	9.2853	9.2853	9.2853	9.2853
	$\overline{b}$	-10	-10	-10	-10	-10	-10	-10	-10	-10	-10
	$\overline{c}$	0.023	0.023	0.023	0.023	0.023	0.023	0.023	0.023	0.023	0.023

Results of Whale Optimization Algorithm:

Optimum strain energy is determined as 241.9811 J for the curvilinear fiber path optimization with the Whale Optimization Algorithm. It is seen that WOA also gives the same global optimum value for the total strain energy and same coefficients for the fiber path definition as the PSO. However, as in the curved panel case, in WOA maximum number of iterations is reached in each run. Optimization details are given in Table 7.

Table 7 - Curvilinear fiber path Whale Optimization Algorithm Results

RUN		**1**	**2**	**3**	**4**	**5**	**6**	**7**	**8**	**9**	**10**
Max. iter #		700	700	700	700	700	700	700	700	700	700
Best Obj. Val.		241.9812	241.9811	241.9816	241.9813	241.9812	241.9818	241.9811	241.9812	241.9816	241.9811
FEA		247.9930	247.9930	247.9930	247.9930	247.9930	247.9930	247.9930	247.9930	247.9930	247.9930
FEA Error		2.48%	2.48%	2.48%	2.48%	2.48%	2.48%	2.48%	2.48%	2.48%	2.48%
Best Var.	$\overline{a}$	9.2853	9.2853	9.2853	9.2853	9.2853	9.2853	9.2853	9.2853	9.2853	9.2853
	$\overline{b}$	-10	-10	-10	-10	-10	-10	-10	-10	-10	-10

	$\bar{c}$	0.023	0.023	0.023	0.023	0.023	0.023	0.023	0.023	0.023	0.023

The resulting optimum fiber path is given in Figure 10. As before, the blue line shows +θ orientation of the fibers, the red line shows –θ orientation of the fibers.

In Figure 10, it seen that the reference fiber path definition is nearly symmetric. Curvature of the curved skin panel is creating the major asymmetry in the reference fiber path definition. Since the loading is slightly asymmetrical, there is still a small asymmetry in the reference fiber path definition. In the future studies, symmetrical loading for the current problem will be assessed. It is expected to have perfectly symmetric reference fiber path definition for the panel.

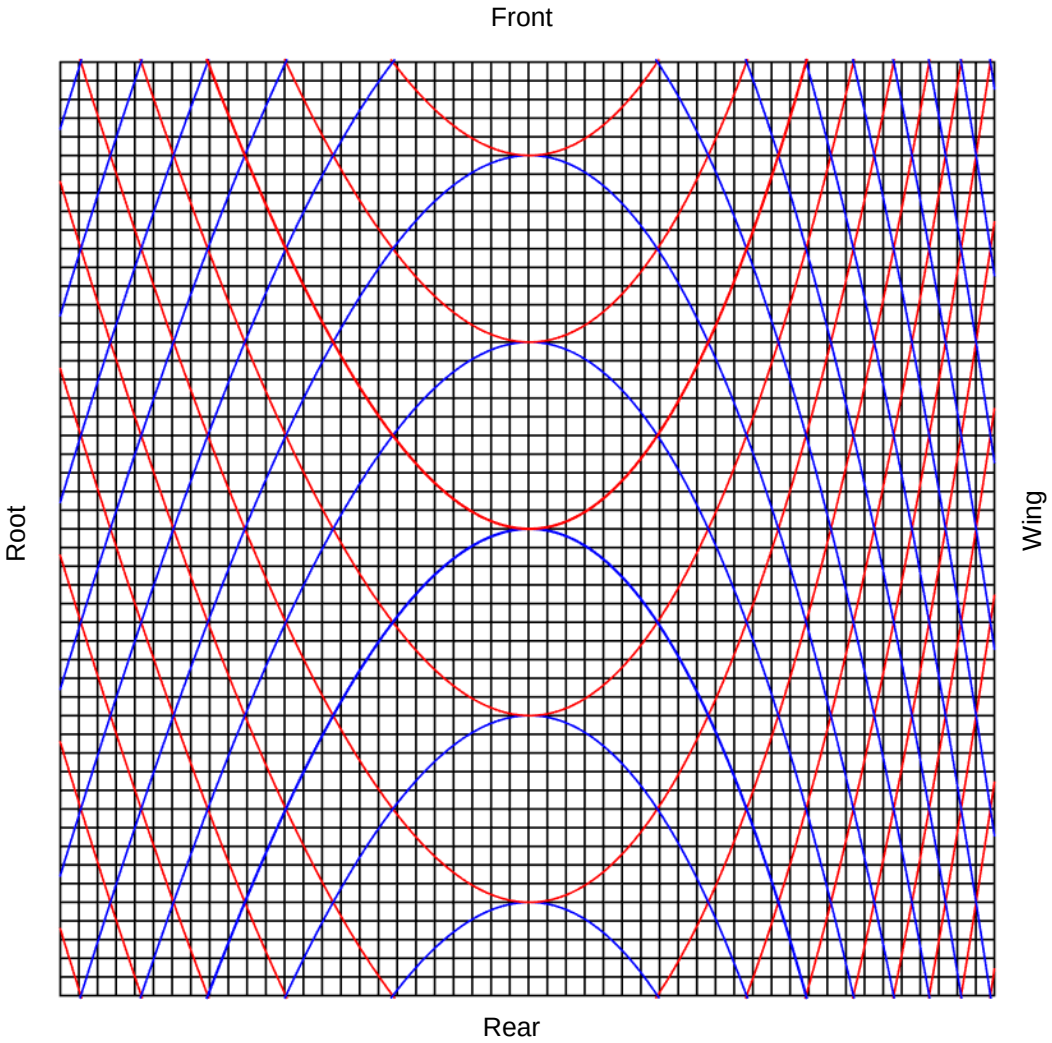

Figure 10 - Resulting curvilinear fiber paths of the flat plate, (top view)

Optimization of Curved Panel with Manufacturing and Failure Constraints

As the third step, optimizations are performed by including both manufacturing and failure constraints utilizing the surrogate models generated for the compliance response and Tsai-Wu failure index. For the surrogate model generation, the optimum parameters used are given in Table 8 and Table 9 for compliance and failure responses, respectively. It should be noted that the same surrogate model for the first set of optimizations is also used for the compliance response. Surrogate model for the Tsai-Wu failure response is created separately for the current optimization study. It is seen that the surrogate model is fitting well

to the finite element model response. The resulting failure value for the first set of model and optimum is 19.3797.

Table 8 - Curvilinear fiber path optimization compliance response surrogate model parameters and performance metrics for the curved panel

# of train. data	**# of ctrl. pnts.**	**Width P.**
600	50	0.2
Rsquare	**RMSE**	**S.average**
0.9387	50.72	609.28

Table 9 - Curvilinear fiber path optimization Tsai-Wu failure index surrogate model parameters and performance metrics for the curved panel

# of train. data	**# of ctrl. pnts.**	**Width P.**
600	50	0.2
Rsquare	**RMSE**	**S.average**
0.9404	1.7548	22.1832

Results of Particle Swarm Optimization:

Ten individual optimization results are given in Table 10. The resulting optimum total strain energy is determined as 808.612 J for the curvilinear fiber path optimization with Particle Swarm Optimization utilizing both the manufacturing and failure constraint. “Best Obj. Val.” is the optimum strain energy obtained from the surrogate model, “Failure” is the maximum failure index obtained from the surrogate model, “FEA” is the finite element analysis solution for the optimum reference fiber path determined, “FEA Failure” is the resultant finite element solution for the maximum failure value, “FEA Error” and “FEA Error F” are the error between the compliance and failure surrogate model response and finite element analysis results, respectively. It should be noted that when failure constraint is added to the optimization problem, the optimum total strain energy increased from 361 J to approximately 809 J.

Table 10 - Curvilinear fiber path Particle Swarm Optimization Results Including Manufacturing and Failure Constraints

RUN		**1**	**2**	**3**	**4**	**5**	**6**	**7**	**8**	**9**	**10**
Max. iter #		468	328	680	487	700	480	352	326	363	687
Best Obj. Val.		808.618	808.612	808.612	808.613	808.618	808.613	808.612	808.612	808.612	808.613
Failure		0.99	1.0	0.99	0.99	0.98	0.99	1.0	1.0	1.0	0.99
FEA		839.623	838.408	839.573	840.318	840.88	839.057	838.623	838.745	839.003	839.231
FEA Failure		1.1073	1.1073	1.1073	1.1073	1.1073	1.1073	1.1073	1.1073	1.1073	1.1073
FEA Error		3.62%	3.55%	3.64%	3.61%	3.71%	3.63%	3.57%	3.56%	3.59%	3.7%
FEA Error_F		10.73%	10.73%	10.73%	10.73%	10.73%	10.73%	10.73%	10.73%	10.73%	10.73%
Best Var.	$\overline{a}$	-8.3312	-8.3311	-8.3313	-8.3311	-8.3311	-8.3311	-8.3311	-8.3311	-8.3311	-8.3311
	$\overline{b}$	0.2173	0.2162	0.2167	0.2162	0.2162	0.2162	0.2162	0.2162	0.2162	0.2162
	$\overline{c}$	1.948	1.9479	1.9477	1.9479	1.9479	1.9479	1.9479	1.9479	1.9479	1.9479

Results of Whale Optimization Algorithm:

Among the 10 individual optimization runs performed with WOA, the resulting optimum total strain energy is determined as 808.612 for the curvilinear fiber path optimization with the Whale Optimization Algorithm including both manufacturing and failure constraints. In the

WOA, the maximum iteration number is used and the 6th optimization run yielded the lowest objective value.

Table 11 - Curvilinear fiber path Whale Optimization Algorithm Results Including Manufacturing and Failure Constraints

RUN		**1**	**2**	**3**	**4**	**5**	**6**	**7**	**8**	**9**	**10**
Max. iter #		700	700	700	700	700	700	700	700	700	700
Best Obj. Val.		810.543	809.327	811.946	808.612	809.634	808.612	811.345	809.612	808.612	810.396
Failure		0.98	0.99	0.98	1.0	0.99	1.0	0.97	1.0	1.0	0.98
FEA		842.845	840.283	845.934	839.723	840.864	838.408	844.864	839.053	838.753	842.295
FEA_Failure		1.1073	1.1073	1.1075	1.1073	1.1073	1.1073	1.1073	1.1073	1.1073	1.1073
FEA Error		3.71%	3.62%	3.68%	3.58%	3.59%	3.55%	3.76%	3.57%	3.58%	3.72%
FEA_Error_F		10.73%	10.73%	10.76%	10.73%	10.73%	10.73%	10.76%	10.73%	10.73%	10.75%
Best Var.	$\overline{a}$	-8.3316	-8.3316	-8.3323	-8.3311	-8.3314	-8.3311	-8.3321	-8.3311	-8.3311	-8.3316
	$\overline{b}$	0.2171	0.2164	0.2161	0.2162	0.2161	0.2162	0.2165	0.2162	0.2162	0.2159
	$\overline{c}$	1.945	1.9474	1.9483	1.9479	1.9475	1.9479	1.9471	1.9479	1.9479	1.9478

Both optimizers reached the same optimum total strain energy and this implies that the optimum total strain energy is actually the global optimum. The resulting fiber path of the optimizations is given in Figure 11. The blue line shows +θ orientation of the fibers, the red line shows –θ orientation of the fibers.

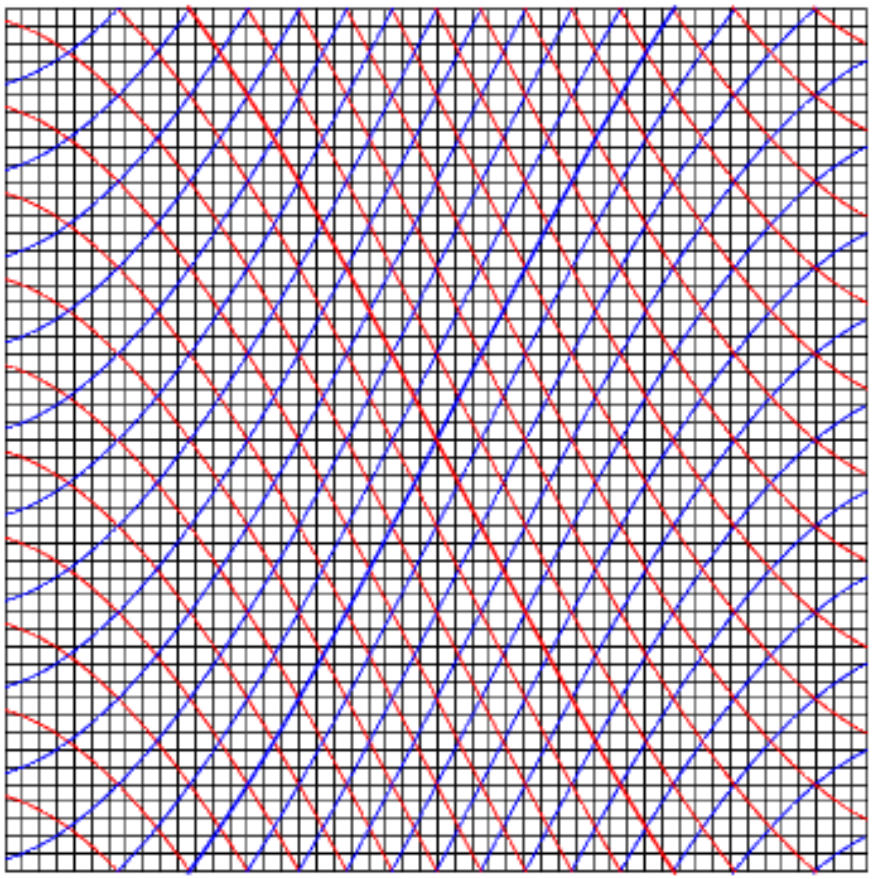

Figure 11 - Resulting curvilinear fiber paths of the curved plate with both constraints, (top view)

As stated earlier, the optimized curved composite skin panel without failure constraint has a maximum failure index of 19.3797. The failure index distribution of the panel is shown in

Figure 12. As seen from Figure 12, failure index is high at the corners of the panel which are the intersection of the skin-rib and spar web panels.

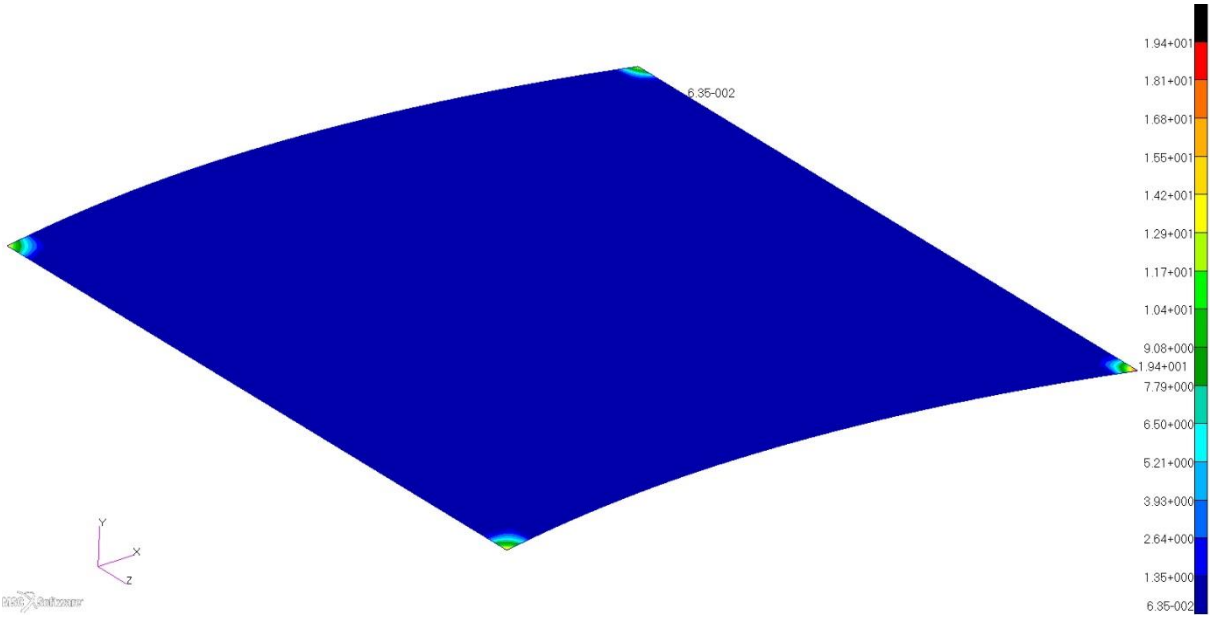

Figure 12 – Failure index distribution of the optimized composite panel without failure constraint

Optimized failure index distribution of the composite skin panel with both manufacturing and failure constraint is shown in **Figure 13**.

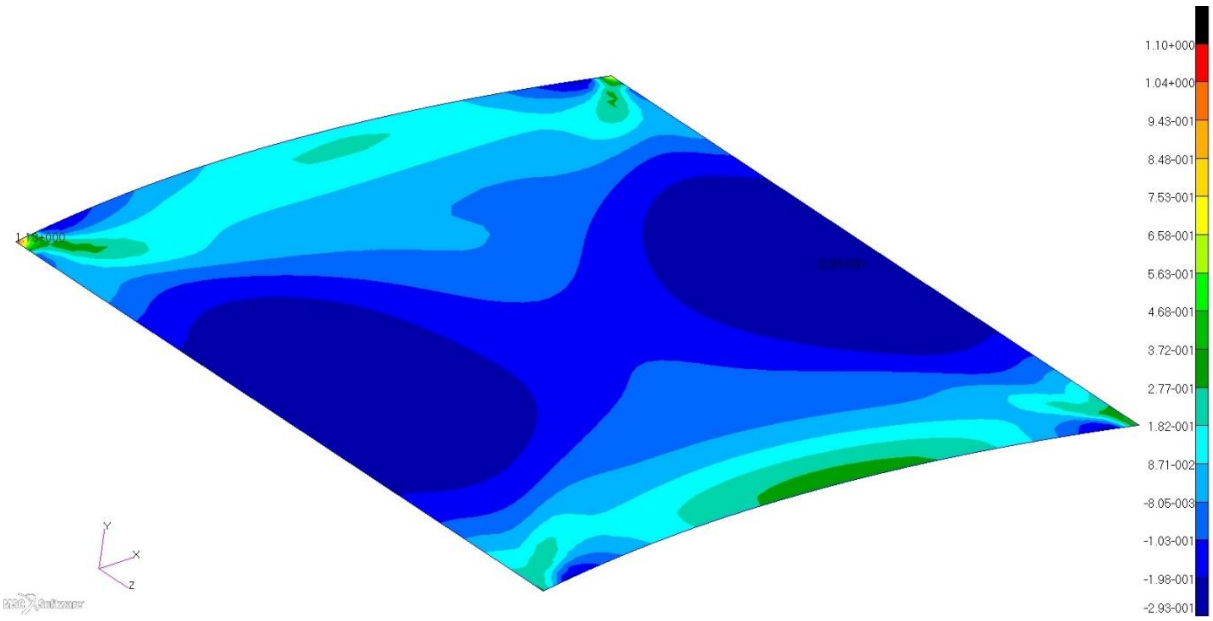

Figure 13 - Failure index distribution of the composite panel with manufacturing and failure constraints

It is seen that by adding the failure index constraint, failure index is distributed more evenly over the panel.

CONCLUSION

In this study, the convenience of the fiber path definition over the 3 dimensional wing skin panel is investigated with real life constraints. The first set of analysis is the basis of the study. In first set of analysis, the fiber path optimization is performed over the curved panel for minimum compliance with the manufacturing constraint only. By checking the results, it is seen as a necessity to assess the performance of the fiber path definition on the skin panel. Therefore, flat skin panel model is prepared to be optimized with only manufacturing constraint. The results are investigated and seen that the resulting fiber paths are reasonable fiber paths over the flat skin panel.

As the third set of optimization, curved skin panel model is optimized by adding the Tsai-Wu failure index constraint, in addition to the manufacturing constraint. For the failure index values, the maximum index is read from the output of the finite element analysis. Separate surrogate model is prepared for the failure response of the problem. Therefore, the optimization is performed with two separate surrogate models for both compliance and failure responses.

In the third set of optimization, total strain energy increased from 361.1 J to 808.6 J, whereas the maximum Tsai-Wu failure index decreased from 19.38 to 1.0. These results are the surrogate model results, except the failure index value for the first set of optimization. Surrogate model errors with respect to finite element analysis for the total strain energy and failure index are 3.55% and 10.73% respectively.

Current study shows that analytical reference fiber path definition over the curved skin panel is convenient to use. The constraints allow the design to be manufacturable, and applicable to real life structures.

References

Blom, A. W., Setoodeh, S., Jan, M. A. M., and Gürdal, Z. (2008) *Design of variable-stiffness conical shells for maximum fundamental eigenfrequency*, Computers&Structures, Vol. 86, pp. 870, 878

Broomhead, D. S. and Lowe, D. (1988) *Radial Basis Functions, Multi-Variable Functional Interpolation and Adaptive Networks,* Royal Signals and Radar Establishment, London

Gürdal, Z. and Olmedo R. (1993) *In-plane Response of Laminates with Spatially Varying Fiber Orientations: Variable Stiffness Concept,* AIAA Journal, Vol. 31, Issue 4

Gürdal, Z., Tatting, B. F. and Wu, C. K. (2008) *Variable stiffness composite panels: Effects of stiffness variation on the in-plane and buckling response*, Composites: Part A, Vol. 39, pp. 911, 922.

Hyer, M. W. and Lee, H. H. (1991) *The use of curvilinear fiber format to improve buckling resistance of composite plates with central circular holes*, Composite Structures, Vol. 18

Lopes, C. S., Camanho, P. P., Gürdal, Z., and Tatting, B. F. (2007) *Progressive failure analysis of tow-placed, variable stiffness composite panels*, Int. Journal of Solid and Structures, Vol. 44, pp. 8493, 8516.

Lopes, C. C., Gürdal Z., and Camanho, P. P. (2008) *Variable stiffness composite panels: Buckling and first-ply failure improvements over straight-fiber laminates*, Computers&Structures, Vol. 86, pp. 897, 907

Nik, M. A.; Fayazbakhsh, K.; Pasini, D. and Lessard, L. (2014) *A Comparative Study of Metamodelling Methods for the Design Optimization of Variable Stiffness Composites*, Composite Structures, Vol. 107, p: 494-501

Olmedo, Reynaldo and Gürdal, Zafer (1993) *Buckling Response of Laminates with Spatially Varying Fiber Orientations*, Proceedings of the 34th AIAA/ASME/ASCE/AHS/ASC Structures, Structural Dynamics and Materials Conference, La Jolla, CA, April 1993

Setoodeh, S., Abdalla M. M. and Gürdal Z. (2006) *Design of variable-stiffness laminates using lamination parameters*, Composites: Part B, Vol. 37, pp. 301, 309

Setoodeh, S., Abdalla M. M., Ijsselmuiden S. T. and Gürdal Z. (2008) *Design of variable-stiffness composite panels for maximum buckling load*, Composite Structures, Vol. 87, pp. 109, 117

Shi, Y. and Eberhart, R. C. (1998) *A modified particle swarm optimizer,* IEEE Int. Conf. on Evolutionary Computation, 1998.

Mirjalili, S., & Lewis, A. (2016). The Whale Optimizaiton Algorithm. (95).

Tatting, B. F. and Gürdal, Z. (2003) *Automated Finite Element Analysis of Elastically-Tailored Plates*, NASA/CR-2003-212679

Waldhart, C. (1996) *Analysis of Tow-Placed, Variable-Stiffness Laminates,* Thesis Submitted to the Faculty of the Virgina Polytechnic Institute and State University, June 5th 1996